Comparison of Single Element Rocket Combustion Chambers with Round and Square Cross Section

S. Silvestri[⋆†], *M. P. Celano*[⋆], *G. Schlieben*[⋆], *O. J. Haidn*[⋆] *and O. Knab*[⋆⋆]
[⋆] *Institute of Flight Propulsion (LFA), Technische Universität München (TUM), Germany*
[⋆⋆]*Airbus Space and Defence, München, Germany*
[†] Corresponding author

Abstract

In the current study, results from an experimental investigation on oxygen/methane single-injector combustion chambers, having round and square cross section, are presented. The commonalities between the combustion chambers in terms of geometries and operating conditions are analyzed in detail. Furthermore several scaling procedures are taken into consideration. The two main scaling criteria applicable for this experimental setup and hardware configuration are theoretically and experimentaly investigated. In development of new combustors, comparisons are often made between predicted performance in a new combustor and measured performance in an other combustor with different geometric and thermodynamic characteristics. Therefore detailed information about thermal loads, combustion performance, as well as pressure and temperature distribution along the chamber wall at representative rocket engine conditions, are presented for the two geometries tested.

Nomenclature

A_s	:	hot wall surface (m^2)	PDE	:	Partial Differential Equation
A_{th}	:	throat area (m^2)	q'	:	heat addition per unit volume (W/m^3)
C_d	:	discharge coefficient	$\dot{q}$	:	heat flux (W/m^2)
c_p	:	specific heat at constant pressure (J/kgK)	T	:	temperature (K)
c_v	:	specific heat at constant volume (J/kgK)	t	:	time (s)
c^*	:	characteristic exhaust velocity (m/s)	u	:	combustion velocity (m/s)
D	:	diffiusion coefficient (m^2/s)	V	:	chamber volume (m^3)
GOX	:	gaseous oxygen	VR	:	velocity ratio methane/oxygen
GCH_4	:	gaseous methane	w	:	thickness of the chamber (m^2)
J	:	momentum flux ratio methane/oxygen	z	:	coord. along chamber axis (m)
L	:	chamber length scale (m)	ϵ_c	:	contration ratio
L'	:	chamber length (m)	γ	:	specific heat ratio
L^*	:	chamber characteristic length (m)	λ	:	heat conduction (W/mK)
LOX	:	liquid oxygen	ρ	:	density (kg/m^3)
OF	:	oxydizer to fuel ratio	μ	:	absolut viscosity (m^2/s)
p_c	:	pressure (bar)			
τ_i	:	characteristic conversion time of chemical species (s)			

1. Introduction

Today's high performance liquid propellant rocket engines for transfer into orbit and space exploration are mostly based on well-established cryogenic propellant combinations like liquid oxygen/liquid hydrogen (LOX/LH2), due to their high specific impulse. The potential of using hydrocarbon as propellant, in particular methane instead of hydrogen, is under active consideration since it could be a solution for the high operational costs. Methane shows, compared to other hydrocarbon fuels, better overall performance from a system point of view,[1] higher specific impulse and simple extractability from natural gases. The design and optimization of liquid rocket engines using methane require a detailed knowledge and understanding of the dominating physical phenomena of propellant injection, combustion

and heat transfer. Already in the '80s, oxygen/methane propellants have been examined for high chamber pressure boost phase engine applications,[2] and this fluid combination has been studied by several research teams in the US Space program[3] as well in Russia[4] and in Europe.[5] Recently, the interest for this propellant combination has arisen. European and Russian industries[6] cooperate to conceive a LOX/CH4 engine for booster applications. Jaxa[7] conducts hot-firing test on a LOX/CH4 rocket engine for an upper stage system. Perdue University[8] focuses the attention on LOX/CH4 expander cycle engines. However, the new propellant combination brings new challenges and the knowledge in oxygen/methane combustion, flame stabilization and injector design criteria need a wide-range of experimental and analytical database.

In the context of the national research program Transregio SFB/TRR-40 on "Technological Foundations for the Design of Thermally and Mechanically Highly Loaded Components of Future Space Transportation Systems", two multi-injector combustion chambers are designed for gaseous oxygen (GOX) and gaseous methane (GCH4). A high pressure combustion chamber (operating from 40 bar to 100 bar), equipped with a round pattern of seven injectors, and a combustion chamber with rectangular cross section for low pressure ranges (10 bar to 40 bar) housing a line of five injector elements, are used. A key aspect of this project is to improve the knowledge on heat transfer processes and cooling methods at representative engine-like conditions, focusing on injector-injector and injector-wall interactions. For this purpose, classical measurement techniques together with inverse methods are used to reconstruct the temperature field in the chamber wall material and the heat flux profile. Furthermore, the low pressure chamber is equipped with a quartz window to allow optical diagnostic techniques. The flat window and the rectangular cross section of the hardware will allow full optical access to the flame interaction, avoiding, compared to a round chamber, the distortion due to the curvatures and the flow disturbances caused by the presence of window corners. In order to profit from the results coming from the optical measurements also for the high pressure level, the two chambers feature the same performance and design parameters , in this way a scalability criterion of the injector can be established. As a first attempt in this direction, two single element capacitive chambers, having either round or quadratic cross section, are build and tested at the Institute of Flight Propulsion. A schematic of possible scaling approaches, the experimental results obtained and the influence on the heat loads and combustion performance for the single element chambers, are the focus of the current research.

2. Similarity parameters and scaling methods

Scaling of combustion devices for Liquid Propellant Rocket Engines is a powerful potential tool for the development of new combustion devices. Today some kind of scaling is used in every development program, essentially when information from a previous program is used to create a new design. More than 50 years ago, Penner[9] obtained a set of similarity parameters for steady internal aerothermochemistry in liquid propellant rocket engine combustion flows by writing the conservation of mass, momentum and energy in a non-dimensional form. The equality of the non-dimensional groups of parameters, which multiply the dimensionless differential equations, assures that the steady aerothermochemical processes are comparable. The set of similarity parameters interesting for the study is given as follow:

$$\text{Reynolds number} = Re = \frac{\rho u L}{\mu} \tag{1}$$

$$\text{Schmidt number} = Sc = \frac{\mu}{\rho D} \tag{2}$$

$$\text{Prandtl number} = Pr = \frac{c_p \mu}{\lambda} \tag{3}$$

$$\text{Mach number} = Ma = \left(\frac{\rho u^2}{\gamma p}\right)^{1/2} \tag{4}$$

$$\text{Specific heat ratio} = \gamma = \frac{c_p}{c_v} \tag{5}$$

$$\text{First Damköhler group} = Da_I = \frac{L}{u \tau_i} \tag{6}$$

$$\text{Third Damköhler group} = Da_{III} = \frac{q' L}{u c_p T \tau_i} \tag{7}$$

The Reynolds number (Re) is the ratio of inertial force to viscous force in the unit volume. It indicates the state of the motion. The Schmidt number (Sc) is the ratio of kinetic viscosity to molecular diffusivity. The Prandtl number (Pr) is the ratio of momentum diffusivity to thermal diffusivity. When identical propellants are used the Pr is kept constant. The Mach number (Ma) is the ratio of kinetic energy of the flow to internal energy. The specific heat ratio (γ) is the ratio of the specific heat at constant pressure to the specific heat at constant volume. The first Damköhler group (Da_I) is the ratio of the convection time rate to the chemical reaction time rate. The third Damköhler group (Da_{III}) is the ratio of the heat addition rate per unit volume by chemical reaction to the rate of removal of heat by convection of enthalpy. While the first five groups are familiar for non reacting flow processes, the Damköhler groups introduce the chemical changes in the flow processes.

Despite the validity of this matematical approach, it is challenging to understand how to determine the rate-controlling steps, which will require a thorough examination of the physical and chemical processes of combustion. Nowadays, two methods are mainly used to scale between full-size combustors and small-sized hardware: the use of identical injector elements and the use of photo-scaled injector elements. Although the photo-scaled-element method offers the advantage of combustion stability information from the scaled combustor test, the identical-element method is preferable for combustion and performance studies, because the injector parameters practically match the full scale and, with proper geometry, the Mach number can be matched as well. Since the injection element itself has the greatest influence on the characteristics of performance, heat transfer, combustion stability and ignition and, due to the fact that combustion stability is not the focus of the research, the injector element is kept the same for the single element combustion chambers as well as for the multi-element chambers. Furthermore, to mantain the mean level of mixing in the developing combustion flow field, the mean value of the Mach number and therefore the contraction ratio of the hardware is identical.

Mantaining full combustion similarity in rocket flow systems is pratically impossible, thus, a partial modelling is necessary. Keeping the geometry similarity previously described, different scaling approaches for the single element chambers are considered. The injector element mass flow can be kept the same for the two hardware. This would result, due to the different throat area, in a variation of the combustion chamber pressure, as well as in a variation of the hot gas velocity in the chamber, which would influence the boundary layer development. When instead the combustion parameters in terms of pressure and mixture ratio are kept the same, the injection conditions are subject to variations that could lead to different injector performances. If, as alternative, the combustion chamber and the injection conditions should be preserved, the mixture ratio or the contraction ratio of the two test hardware need to be modified. This would affect the characteristic velocity in the chamber, hence the performance characteristics. Due to the ignition limits of methane/oxygen combustion on one hand, and exceeding the stoichiometric mixture ratio on the other hand, the variation of mixture ratio, necessary to mantain the same combustion chamber pressure and the same injection conditions, can not be achieved in the range of mixture ratios experimentally tested. Moreover, since the final scope of the research is the characterization of the multi-element chambers, the chamber geometry is not further modified and the latter case is not analyzed.

3. Test specimen and experimental configuration

All the experiments have been performed at the Institute of Flight Propulsion's test facility at the Technical University of Munich (TUM). The movable test bench allows experiments with gaseous methane and gaseous oxygen for designed interface pressures up to 50 bar. In this section a description of the single element rocket combustion chambers having rectangular and round cross section, the injector geometry, the measurement equipment and data analysis procedures is presented.

3.1 Hardware description

The investigations are performed using two modular capacitive cooled combustion chambers having round and square cross section. The combustion chambers are designed for a testing time of up to 4 s at a pressure of 20 bar and mixture ratio of 3.4. The inner chamber dimensions are shown in Table 1.

The round combustion chamber, depicted in Fig. 1(a), features an inner diameter of 12 mm and a conical nozzle with a throat diameter of 7.6 mm. The rectangular chamber instead, shown in Fig. 1(b), has an inner square cross section of 12 mm x 12 mm and a truncated trapezoidal nozzle with a rectangular throat section of 4.8 mm x 12 mm. The chamber height is kept identical in order to provide the same injector wall distance of 3 mm. A Mach number of 0.24, typical for rocket applications, is achieved by a contraction ratio of 2.5 for both chambers. All chamber segments are made of oxygen-free copper (Cu-HCP).

The injector head of the combustors is designed to allow different injector designs. For the current study, a single shear coaxial injector element is used. Table 2 shows the main characteristic dimensions of the injector. To center the

Table 1: Combustion chamber dimensions

		Rect. comb. chamb.	**Round comb. chamb.**
Chamber length[a]	[m]	$290 \cdot 10^{-3}$	$285 \cdot 10^{-3}$
Chamber width	[m]	$12 \cdot 10^{-3}$	-
Chamber height	[m]	$12 \cdot 10^{-3}$	-
Chamber diameter	[m]	-	$12 \cdot 10^{-3}$
Throat diameter	[m]	-	$7.6 \cdot 10^{-3}$
Throat height	[m]	$4.8 \cdot 10^{-3}$	-
Throat width	[m]	$12 \cdot 10^{-3}$	-
Throat area	[m^2]	$57.6 \cdot 10^{-6}$	$45.4 \cdot 10^{-6}$
Contraction ratio A_{cc}/A_{th}	[-]	2.5	2.5

[a] Length of the cylindrical part

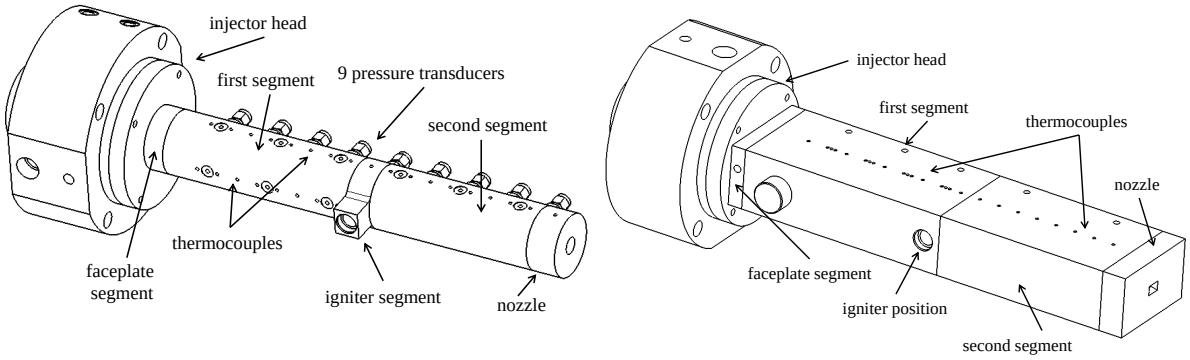

(a) Round combustion chamber

(b) Rectangular combustion chamber

Figure 1: Combustion chamber schematics

injector element in the faceplate, the GOX tube is equipped with four equally-spaced fins. For the current test series, the fins are positioned with an angle of 45° to the temperature measurement center plane. To ensure homogeneous injection conditions in terms of temperature and pressure, two porous plates are placed in the oxidizer and fuel manifolds. A scheme of the injector design is shown in Fig. 2.

Table 2: Injector dimensions

GOX inner diameter	d_i	[m]	$4 \cdot 10^{-3}$
GCH4 outer diameter	d_o	[m]	$6 \cdot 10^{-3}$
GOX tube wall thickness	t	[m]	$0.5 \cdot 10^{-3}$
GOX tube length	l	[m]	$96 \cdot 10^{-3}$
Injector area ratio	A_{GCH4}/A_{GOX}	[-]	0.7

3.2 Experimental setup

Both the hardware are equipped with standard instrumentation required to characterize the operation of the combustion chamber. For a better understanding of the complex heat transport processes, equally spaced pressure transducers on the side wall provide a well resolved measurement of the wall pressure distribution $p(z)$ along the chamber. The *WIKA A10* pressure sensors are individually calibrated and operated at a data acquisition rate of 100 Hz. To characterize the injection conditions, thermocouples of type K with 0.5 mm diameter, and pressure transducers are installed in the chamber manifolds, prior the porous plates. A scheme of the combustion chambers and the associated sensor locations is given in Fig. 1. To determine the temperature field within the chamber material, type T thermocouples of 0.5 mm diameter are mounted with a regular path along the center plane of both the combustion chamber with a distance

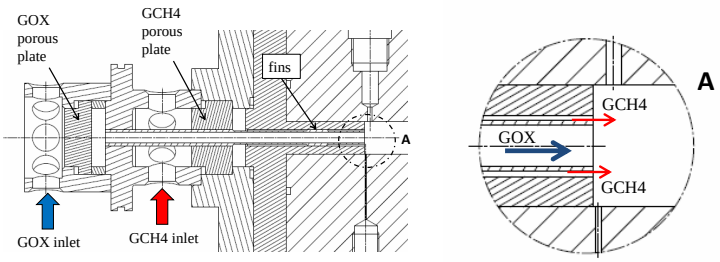

Figure 2: Single shear coaxial injector

of 1 mm from the hot wall. Additionally, in the first segment of the round combustion chamber, thermocouples are mounted at 3 mm distance to the hot wall at the same axial positions of the other measurement points, but with an angle of 90°. In the first segment of the rectangular chamber, instead, the thermocouples are located at 2 mm and 3 mm distance from the hot wall on the central plane, shifted by 3.5 mm steps along the chamber axis. In both chambers the pressure transducers, as well as the thermocouples placed at 1 mm from the hot wall, present the same axial pitch of 34 mm and 17 mm respectively. Further information about the hardware setup for the rectangular and round combustion chamber can be found in previous publications.[10,11] A spring loaded system, providing a constant force of about 2 N,[12] ensures a continuous contact between the thermocouple's tip and the base of the hole. The thermocouple location pattern is shown in Fig. 3.

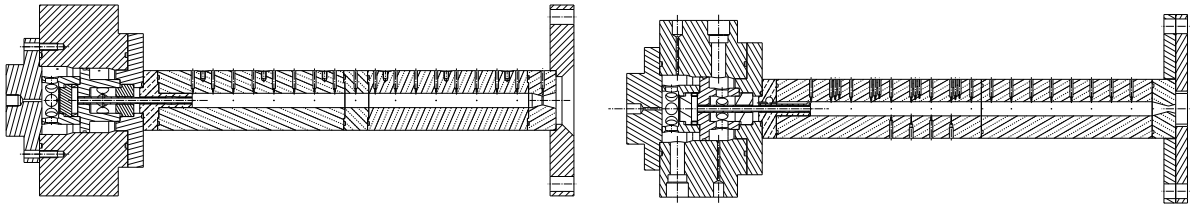

(a) Round combustion chamber

(b) Rectangular combustion chamber

Figure 3: Thermocouple positions at 1 mm along the combustion chamber axis

3.3 Operating conditions

The ignition of the chambers is achieved by a torch igniter using gaseous methane/gaseous oxygen, which is mounted in a central axial position. The mass flow rates in the combustion chamber (GCH4, GOX, GN2 for purge) are set by sonic orifices in the feed lines and the corresponding upstream pressure. The orifices in the feed lines to the main injector are manufactured with appropriate diameters and calibrated prior to the test campaign with gaseous nitrogen using a Coriolis flow meter. In order to increase the accuracy of the calculated mass flow rates, the value of the discharge coefficient (C_d) is implemented in the evaluation routine as variable function of upstream temperature and pressure.[13] The burning time is kept constant for all the tests to 3 s and the same hot run sequence between the test campaigns has been used. With regards to the two scaling methodologies selected for the current work, two test matrices are established. For the first scaling approach, the same pressure in both the chambers is maintained constant for the two test set-up and tests were performed at 10 and 20 bar chamber pressure and mixture ratios that vary from 2.2 to 3.4. The test matrix for this scaling approach is given in Fig. 4(a). For the second scaling approach, the mass flow rate at the injector is preserved. Due to the smaller throat area of the round combustion chamber, higher pressure levels, of 12 and 25 bar, are achieved for this chamber configuration when operated at the same mass flow rate as the rectangular chamber. The injected mass flow for the different mixture ratios tested is presented in the test matrix in Fig. 4(b).

4. Experimental results and discussion

The main goal of the research is to characterize and compare the injector behavior in terms of heat loads to the wall and performance parameters for the different scaling procedures. In the present paragraph the pressure and temperature

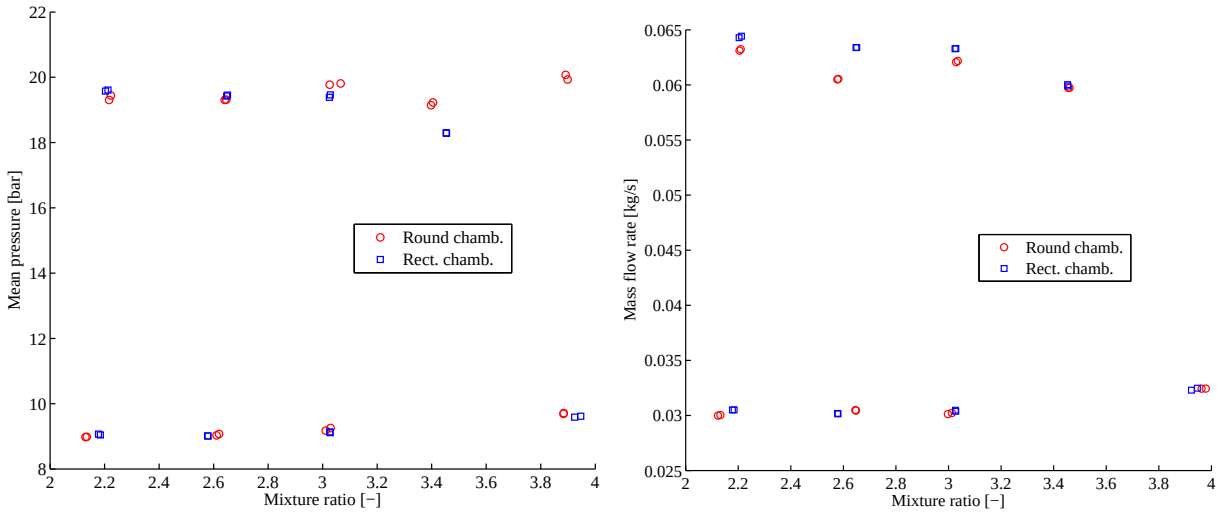

(a) Constant combustion chamber pressure

(b) Constant mass flow rate

Figure 4: Operating points for the scaling approaches

load distribution along the combustion chambers main axis as well as the heat loads and combustion efficiency for the two scaling methods are presented. Due to the transient behavior of the hardware, three time intervals are defined for the evaluation of the test data (see Fig. 5): a time interval t_0 for initial conditions, a time interval t_1, named evaluation time, characteristic for the hot run, and a time interval t_2 for shutdown conditions. The time t_1 is taken at 2/3 of the hot run. To minimize the influence of the transient start up, the performance parameters as well as temperature, pressure and the heat flux distribution along the combustion chamber axis are calculated as mean values over a 0.5 s time interval at the evaluation time. A different approach is followed for the evaluation of the combustion chamber pressure distribution. To reduce possible deviations coming from signal noise, a piecewise linear fit is applied on the pressure signal. Data presented in the following section are obtained as the mean value of a single load point and its repetition. Due to the good matching of the nominal and the actual load points, the 20 bar OF=2.2 and OF=3.0 tests and the 20-25 bar OF=2.2 and OF=3.4 tests respectively, are chosen as examples of the test results for the first and second scaling approach.

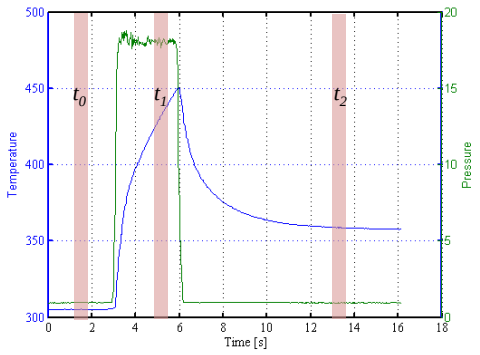

Figure 5: Temperature and pressure profile

4.1 Influence of combustion chamber geometry

One of the influencing parameter for the performance in the combustion chamber, it is the geometry of the chamber itself. While comparing the two set-ups the difference in geometries has to be taken into account. The two most important features of the combustion chamber are its length and its shape. In order to isolate the effects resulting from the different shapes and to minimize the differences of the upcoming multi-element injector chambers, most of the geometry parameters are kept similar between the different hardware. The length of the combustion chamber affects

the overall vaporization efficiency, in case of liquid propellants, and the overall mixing efficiency. For mixing-limited combustion, increasing the chamber length can increase the overall performance but often at a much slower rate, depending on the injector element design. Injector elements that have a higher initial interpropellant mixing, such as coaxial element patterns, show little mixing improvement with increased chamber length.[14] As already described in paragraph 3.1, the two chambers use the same injector design and have the same contraction ratio. In this way, the mean level of the mixing process in the developing combustion flow field is kept similar. Furthermore, a trade-off to keep a similar chamber length and characteristic chamber length, for which the residence time of the propellants in the combustion chamber is determined, has been achieved. An overview of the common parameters is given in Table 3. Moreover, the difference in the pressure losses due to friction and heat losses to the chamber wall are minimized for the two chambers by mantaining the same hydraulic diameter and the volume to surface ratio (V/A_s).

Table 3: Common geometrical parameters of the hardware

			Rect. comb. chamb.	**Round comb. cham.**
Hydraulic diameter	d_{hyd}	[m]	$12 \cdot 10^{-3}$	$12 \cdot 10^{-3}$
Chamber length	L'	[m]	$290 \cdot 10^{-3}$	$285 \cdot 10^{-3}$
Chamber characteristic length	L^*	[m]	$724 \cdot 10^{-3}$	$749 \cdot 10^{-3}$
Maximum chamber wall thickness	w	[m]	$36.5 \cdot 10^{-3}$	$19 \cdot 10^{-3}$
Volume to area ratio	V/A_s	[m]	$3 \cdot 10^{-3}$	$3 \cdot 10^{-3}$
Contraction ratio	ϵ_c	[-]	2.5	2.5

Although most of the geometric parameter are maintained similar, the main difference between the two chambers is the different thickness of the chamber walls and consequently the mass of the combustion chambers. The mass of the rectangular chamber is almost two times heavier than the mass of the round combustion chamber. The main effect coming from the bigger amount of material is visible in the temperature readings. Fig. 6(a) shows the temperature profile for the whole testing time of the rectangular (in red) and round (in blue) combustion chamber at two different axial positions. The termocouples installed at z=0.0855 m (z=0 m at the faceplate) in the first segment are represented by the dotted lines, while the thermocouples in the second segment (at z=0.2215 m) are represented by the solid lines. At the start-up, when the heat wave has not reached the external surface yet, the difference in the slope of the temperature profile depends only on the different surface available. Later on, the havier mass of the rectangular chamber acts as a heat sink and decreases down the steepness of the curve. A big difference is also visible after the shutdown. While in the rectangular chamber the temperature of the material cools down quickly, the round chamber wall remains hotter. In Fig. 6(b), the slope (dT/dt) of the aforementioned temperature profiles is given only during the burning time. At the starting time, the rectangular chamber shows a higher slope. After the thermal wave has come to the external wall, the slope tends to decrease constantly and reaches lower values than in the round combustion chamber. Although the temperature profile in the first and second segments appears almost parallel for the round combustion chamber, the rectangular chamber shows a difference between the two segments, which proceeding with time, that could be due to axial heat flux in the chamber wall or to a different distribution of the boundary layer caused by the chamber corners.

4.2 First scaling approach: similarity in combustion chamber pressure and mixture ratio

The first scaling approach adopted consists in maintaining combustion chamber pressure and mixture ratio constant in both combustion chambers. The two combustors feature the same propellant chemistry, flow mixture ratios and propellant inlet temperatures. Therefore, the Schmidt and the Prandtl numbers are kept constant. Furthermore, having the same combustion chamber pressure, mixture ratio and Mach number in the chamber, results in identical hot gas velocities. With these hypotheses and combinig the Reynolds and the Damköhler numbers, it is possible to obtain a scalability criterion for the chemical conversion time. This approach, also followed by Penner is known as "The Penner-Tsien Scaling Rule".[9] The Reynolds number in the combustion chamber depends mainly on the hot gas properties, the combustion hot gas velocity and the chamber length scale. Thus the Reynolds number, for each hardware, would differ only for the chamber length scale. Since for the case studied, as seen in section 4.1, the length scale, equal to the hydraulic diameter for the rectangular chamber, and to the geometrical diameter for the round chamber, is equal, also the Reynolds number does not differ for the two compared chambers. By coupling the Da_I number with the Re number in Eq. 8 it is possible to conclude that the chemical reaction time in the hardware setups is the same.

$$\frac{\tau_{i,round}}{\tau_{i,rect.}} = \left(\frac{L_{round}}{L_{rect.}}\right)^2 = 1 \tag{8}$$

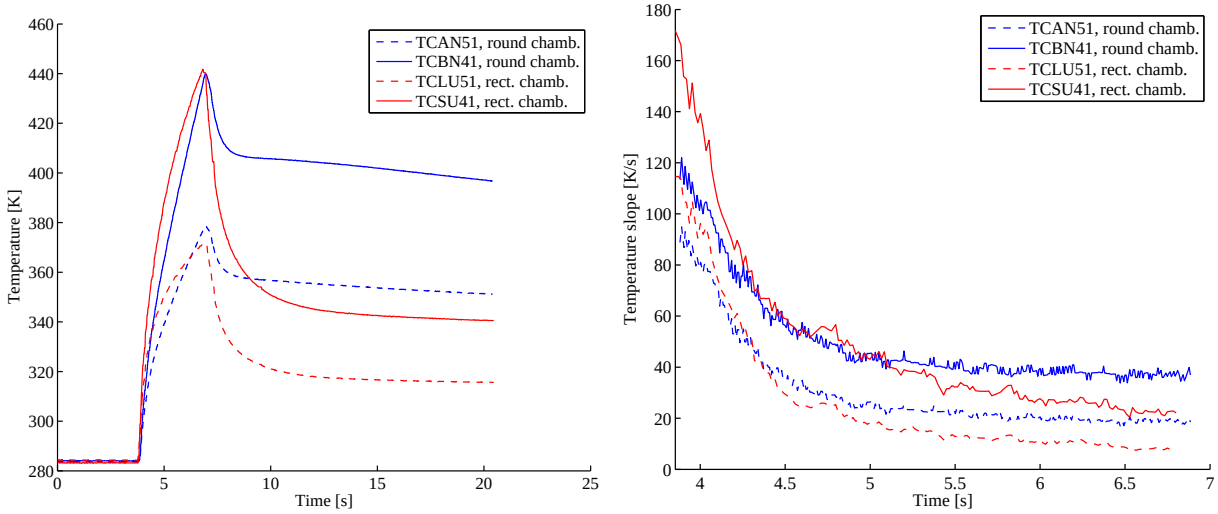

(a) During the whole test duration

(b) During the burning time

Figure 6: Temperature distribution in (a) and slope of the temperature (dT/dt) in (b)

Considering that the residence time of the propellants in the chamber are almost identical due to the similar characteristic length, the combustion processes and in particular the heat release should be alike and consequenthly the pressure decay along the combustion chamber axis is also similar. Fig. 7 shows the comparison of the wall pressure distribution for the round and the rectangular chamber at 20 bar. On the left side, the comparison is shown for a mixture ratio of 2.2. The plot on the right side shows the comparison for a mixture ratio of 3.0. The pressure signal is normalized with the mean chamber pressure in the chamber of each test and its repetition.

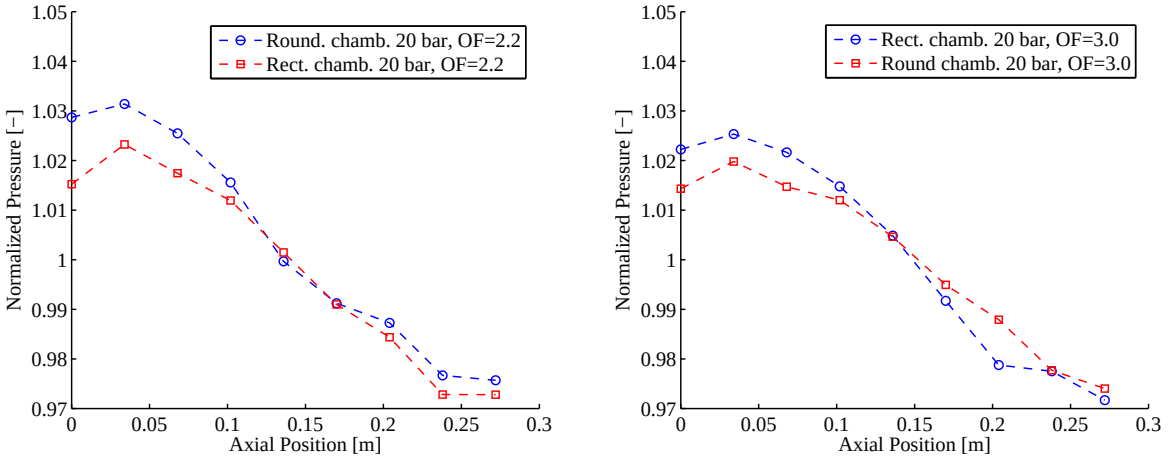

(a) OF=2.2

(b) OF=3.0

Figure 7: Pressure distribution along the chamber axis at p_c=20 bar

Due to the combustion processes, the injected mixture accelerates from the injection velocity to the hot gas velocity for a full combusted flow. Consequently, the wall pressure decreases along the chamber axis and the pressure gradient tends to flatten when the completeness of combustion is reached.[15] A pressure gradient of up to 5% is visibile for both the chambers until the combustion process is accomplished, shortly before the nozzle section. No considerable difference could be seen in the pressure decay for the different pressures and mixture ratios. In the region close to the faceplate a drop in wall pressure, linked to the presence of a recirculation zone, is observable. The stagnation point, shown by the pressure peak, occurs for both the hardware at the same axial position. For the rectangular combustion chamber, where the presence of the corners leads to a bigger volume and the injected velocity is slightly higher, the

effect appears to be stronger and a higher initial rise of the pressure can be seen. For lower mixture ratio cases, when the velocity and the momentum flux for the methane is greater, the difference in the recirculation zone seems to be amplified. In the region close to the injector, the influence of a round flame in a rectangular chamber is more evident, since the flame is not yet complitely adapted to the rectangular shape. This could also cause the flatter shape of the pressure profile along the chamber axis in the first third part of the chamber.

The characteristic of an injector element is mainly defined by the heat loads to the hot wall. The mixing mechanisms in the near injector region determine the flow conditions and influence the flame behavior. Because of the different cross sectional areas of the chamber and the identical contraction ratio, the injected mass flow needs to be scaled proportional according to Eq. 9, to achieve the same combustion chamber pressure level. This however leads to different injection conditions in the two chambers, described later.

$$\dot{m} = \frac{p_c \cdot A_t}{c^*} \tag{9}$$

Due to the gaseous form of the propellants, the variation in the injector velocities is moderate. A maximum difference in velocity of 14% higher for the rectangular combustion chamber is reached. Additionally, the values of the velocity ratio (VR) and the momentum flux ratio (J) vary with OF in small ranges and there is no significant difference for the two chambers. Table 4 gives an overview of the actual variation of VR and J at 20 bar for the different mixture ratios tested. Since for a shear coaxial injector the mixing process increases with fuel to oxidizer momentum flux ratio, similar injector performance has to be expected in both configurations.

Table 4: Velocity ratio and momentum flux ratio for 20 bar case test conditions

	VR				**J**			
Mixture ratio (OF)	2.2	2.6	3.0	3.4	2.2	2.6	3.0	3.4
Rectangular comb. chamb.	1.12	1.03	0.96	0.93	0.74	0.56	0.46	0.39
Round comb. chamb.	1.22	1.05	0.96	0.93	0.80	0.58	0.46	0.40

Despite a different total amount of propellant is injected, the energy per unit volume introduced in the systems remains constant since compensated by the difference in volume of the hardware. The heat transfer, driven by the convection mechanism in the chamber, are similar as long as the Re number and the Pr number are kept constant. Consequently, the rate of heat addition per unit volume by chemical reaction and the rate of heat removed by the convection of the enthalpy are in the same relation and the Da_{III} is also preserved. Keeping of complete chemical and reaction kinetic similarity in the gas stream automatically satisfies the boundary conditions for heat transfer to the chamber wall. For the underlying physical phenomena, the heat flux in the two combustion chambers, is expected to be comparable.

4.2.1 Axial heat flux and temperature distribution

Due to the capacitive design of the hardware, heat fluxes can only be calculated from wall temperature measurements. Several methods to calculate the heat fluxes are investigated at the Institute of Flight Propulsion. In this section an Inverse method using Finite Difference Scheme is briefly described and the test results are analyzed. Detailed information about the heat flux calculation methods can be found in Celano et al.[16]

For the calculation of the heat flux based on the thermocouple measurements, an inverse computational method has been employed. The applied tool relies on an iterative regularization method, which aims to minimize a residual function.[17] In this case, the residual function is defined as the difference between measured and calculated temperature values. To achieve that, the code takes advantage of the variational formulation of the heat diffusion PDEs, leading to a constrained minimization of the residual function. The boundary condition in the chamber wall is represented by the unknown heat flux (over time and position). By using the boundary condition as a necessary optimality requirement, Lagrange multipliers are introduced for the formulation of the residual gradient. Finding the optimal solution corresponds to the minimization of the residual gradient and for this task, the conjugate gradient approach is utilized. This updates the values of the heat flux in each node for the next iteration step. A numerical implementation using the Finite Difference Scheme has been carried out and the tool has been optimized for the combustion chamber geometries. For the round combustion chamber, the modeling domain is defined as a $3D$ cylinder, whereas for the rectangular one, the domain is modeled by a cave square prism. Each computational node is assigned with a value of temperature and heat flux. Since the method involves an iterative solution, the direct problem is solved each time with the new heat flux as boundary condition. Upon convergence, a complete time dependant profile for the heat flux and the temperature is obtained for all points in the domain. The results obtained for the 20 bar case, OF=2.2, on the left, and OF=3.0, on the right, at the evaluation time are reported in Fig. 8.

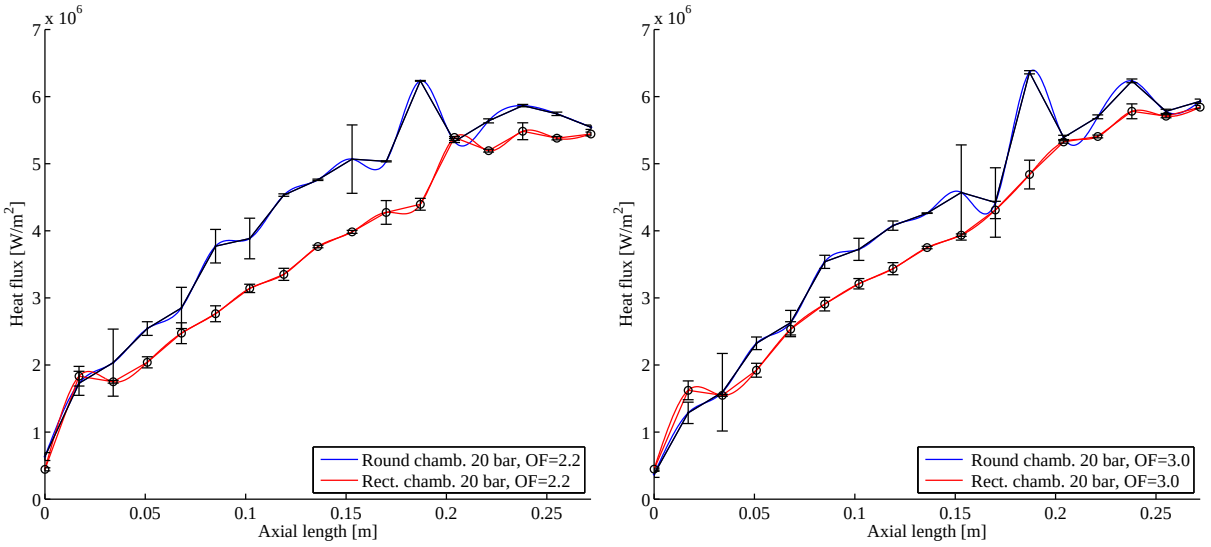

(a) OF=2.2 (b) OF=3.0

Figure 8: Axial heat flux distribution at p_c=20 bar

The wall heat flux versus axial location profile shows, for both combustion chambers, a relatively slow, but steady rise up to a maximum of 6 MW/m^2 just close to the nozzle section. As already seen in previous studies, using a single element rocket combustion chamber with LOX/GCH4,[3] the peak in wall heat flux for shear coaxial injector show in a downstream position. Different behavior instead has been encountered for a swirl coaxial injector, where the heat flux peak is more close to the injector faceplate. Although the maximum heat flux level is comparable for the different hardware configurations, the heat flux of the rectangular chamber (red line in Fig. 8) presents a slightly lower heat flux in the second third of the chamber, this could be attributed to a lower mixing efficiency due to the presence of the corners and to the different recirculation zones. This discrepancy, infact, seems to be stronger for the lower mixture ratio case, where the impact of the recirculation zone is bigger in the rectangular chamber, already visible in the pressure profile in Fig. 7. The recirculation zone affects the local mixing in the near injection region. The burned propellants are transported towards the gaseous methane entering the chamber through the outer injector annulus and have a strong influence on the gas composition near the walls. Therefore the local mixture ratio and the heat conductivity of the gas are not equal to the other chamber anymore. The heat flux, in this region, is then dominated by the creation of recirculation vortices amplified by the bigger volume of the the rectangular chamber. The better mixing in the recirculation zone appears, nevertheless, to be only local and the mixing of the remaining species could lead to a smaller heat flux level in a further downstream position. Furthermore, a not uniform distribution of the heat flux profile in circumferential direction could decrease the annular average level for this chamber configuration, shown in Fig. 8. With increasing mixture ratio, a slight increase in the heat flux can be noticed for both the combustion chambers. The small heat flux peak, in the round chamber, located at z=0.1875 m, is considered to be due to a characteristic behavior of the temperature sensor located at this axial position. Analysis of other tests has led to the conclusion that this peak is independent of the pressure level and the mixture ratios used. The error bars, placed at each measurement position, represent the relative deviation of the calculated heat flux. It is based on a direct solution from a CFD analysis, for which the residual of the calculated and measurement temperature are taken into account.

Due to steady combustion, the temperature increases continously along the chamber axis until the accomplishment of the reaction process. The temperature distribution along the chamber axis ($\Delta T(z)$) for the complete set of thermocouples positioned at 1 mm distance from the hot gas is shown in Fig.9 for both configurations. In a heat sink hardware, higher initial temperature of the test would lead, for the same test duration, to higher levels of temperature. For this reason, only the temperature difference between the signal at the evaluation time (t_1) and at the initial time (t_0) is taken into account. All curves present a steady rise along the chamber axis until z=0.240 m and a short plateau is identified in the last section, close to the nozzle, as indication of end of the reaction process. Although any visible change on the tendency between the chambers for mixture ratio or pressure variations is observed, the temperature level increases for both cases, as already seen for the heat flux analises with increasing mixture ratios.

Due to the different heat capacity of the chambers, an equal heat rate distributed on the hot gas surface would lead to a higher temperature level for the chamber having less mass to disperse the heat, if an equal heat up of the

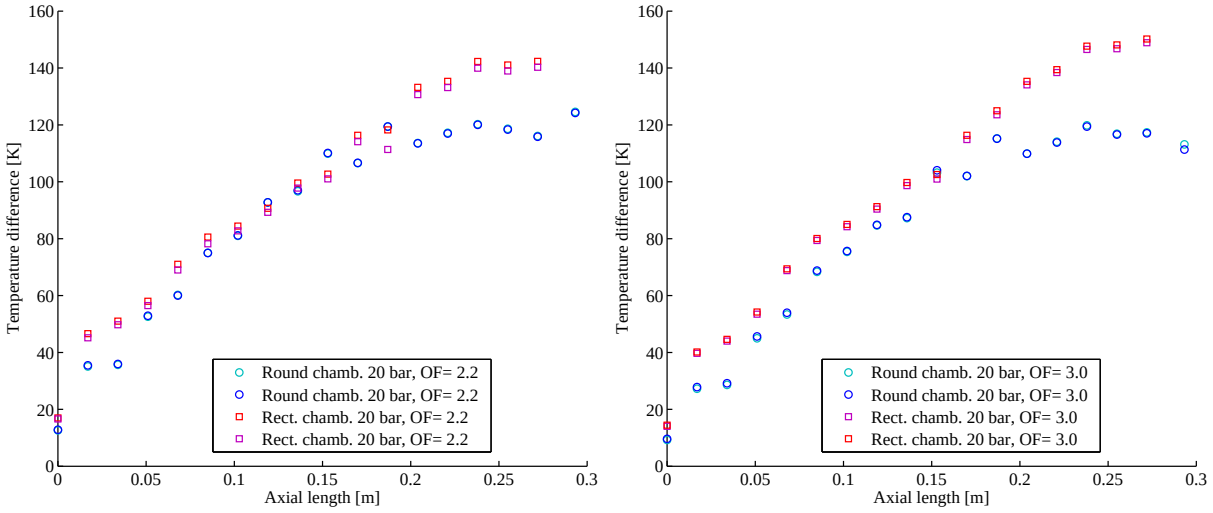

(a) OF=2.2 (b) OF=3.0

Figure 9: Wall temperature distribution at p_c=20 bar

chamber wall material is considered. Therefore, a higher temperature level would have been expected for the round combustion chamber. From the experimental results, instead, a different tendency has been observed. The temperature level of the rectangular chamber (in red) is higher than the one of the round chamber. This behavior can be explained by considering the difference between the internal goemetry of the chambers. For a similar heat flux distribution, the difference in cross sectional area would lead to higher heat rate in the rectangular chamber, since a larger hot gas surface has to be taken into account. The higher heat rate leads, due to the same material properties, to higher temperature level in the rectangular chamber. Furthermore the effect of having a round flame in a square cross section can not be neglected. The heat flux profile will have a maximum on the symmetry plane, where the flat walls are closest to the injector element. Since the thermocouple positions are located on the symmetry plane, this would cause higher temperature readings for the rectangular chamber. This hypothesis is confirmed by having a closer look to the inner surface of the rectangular chamber after the test campaign. The color of the inner wall in circumferential direction is not uniform. The central parts are brighter than the color in the four corners, which corresponds to a higher level of the temperature color scale. CFD simulations, ongoing at the Institute, have already confirmed this behavior. Moreover, the non uniform distribution of the heat flux results in a smaller average heat flux value for the rectangular combustion chamber, when compared to the average heat flux of the round chamber.

4.3 Second scaling approach: similarity in mass flow rate and mixture ratio

In the second scaling approach, the mass flow rate and the mixture ratio are maintained similar in the chambers. Because the contraction ratio has already been fixed and the chamber pressure increases linearly with increasing propellant mass flow rate, see Eq. 9, the resulting combustion chamber pressure in the round chamber is higher than in the rectangular one, see paragraph 3.3. The velocity at the injection, due to the gaseous form of the propellants, decreases with the increase of propellant injection density, which as first approximation, is considered directly proportional to the combustion chamber pressure at the injection exit plane. Hence, the Reynolds number in the injector element and the Reynolds number in the combustion chamber are not constant between the combustors. The difference in the hot gas velocity is, nevertheless, for the variation in pression obtained, less than 0.2%. The chemical reaction time is still dominated by the momentum flux ratio and the velocity ratio at the injection. For this reason the convective transport in axial direction is not dominant and the small energy difference introduced in the system, by the higher propellant density, does not play a role. Further, in this scaling approach, the axial heat release is expected to be similar for both the configurations and no significant difference in the pressure decay along the combustion chamber axis is awaited. Fig. 10 shows the comparison of the normalized wall pressure distribution for the round and the rectangular combustion chambers at $20-25$ bar and mixture ratio of 2.2, on the left, and 3.4, on the right. In this scaling approach no significant variation in the pressure signal can be seen. The wall pressure decreases along the axial direction and a similar pressure decay can be noticed for both combustion chambers. The flattening of the pressure gradient, visible for the lower mixture ratio case, is not so evident for the higher mixture ratio, where the momentum flux ratio tends to diminish.

Furthermore, the pressure peak, due to the recirculation zone, in the round combustion chamber, is smoothing down with higher mixture ratios, where the velocity of the external methane jet is less dominant when compared to the inner oxygen jet.

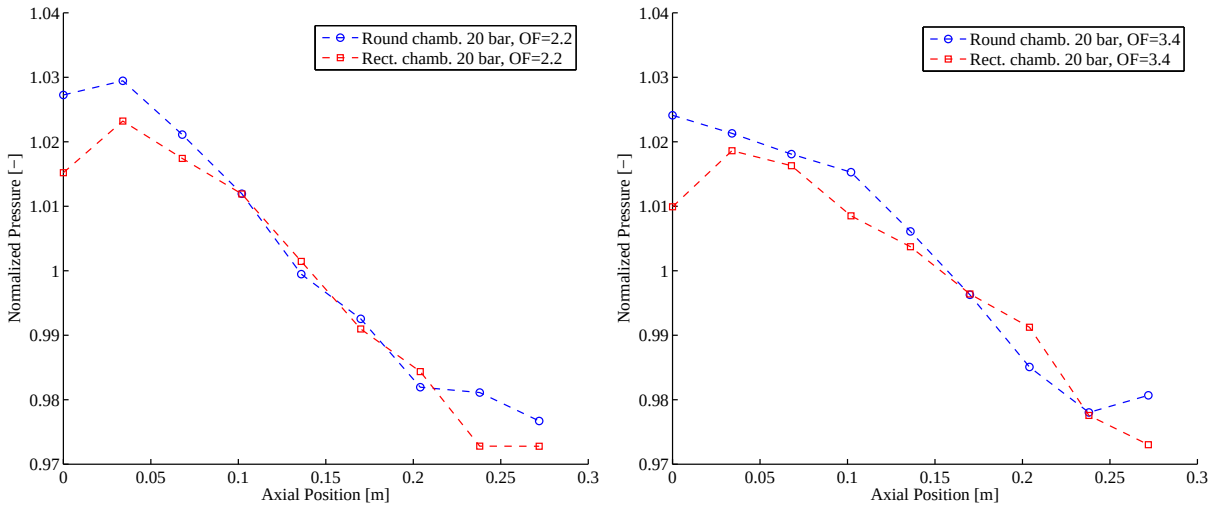

(a) OF=2.2 (b) OF=3.4

Figure 10: Pressure distribution along the chamber axis at p_c=20 bar and p_c=25 bar, respectively for the rectangular and round chamber

4.3.1 Axial heat flux and temperature distribution

Heat transfer correlations available in literature such as Bartz[18] or Dittus Boelter[19] indicate that the heat transfer coefficient is proportional to the pressure to the power of 0.8. The heat flux in the combustion chamber can be seen as the product of the heat transfer coefficient and the temperature difference between the combustion products and the wall. For all cases analyzed, the combustion core temperature is much higher than the measured axial wall temperature. As a first approximation, the wall heat flux should also scale with the combustion pressure as in Eq. 10.

$$\dot{q} \propto P_c^{0.8} \tag{10}$$

Studies with LOX/CH4[3] have shown that for liquid-gas injectors where the fuel to oxydizer momentum flux ratio decreases with chamber pressure, the resulting coupled atomization/mixing/combustion phenomena do not scale simply with pressure, while for a gas-gas injector, where the momentum flux ratio remains nearly constant, this scaling procedure shows good results. Studies[20] on gaseous oxygen-gaseous hydrogen single coaxial injectors confirm that the heat flux of a gas-gas injector combustor correlates well with the pressure as in Eq. 10, as long as the simple scaling criterion of inner combustion flow field is satisfied. Similarity of the main combustion flow field is independent of the Reynolds number for a sufficient turbulent flow in LPREs. Though different *Re* number can produce local quantitavely dissimilar heat transfer and boundary layer flow structure, it still can not avoid the existance of the qualitative similar heat transfer distribution on the combustor wall. The resulting axial profile of wall heat flux will be different between the two chambers and higher heat flux is expected for higher chamber pressure levels. Injecting a total mass flow of about 60 g/s, leads to a chamber pressure of 20 bar in the rectangular chamber and approximately 25 bar in the round one. The results obtained with the Inverse method using a Finite Difference Scheme for OF=2.2, on the left, and OF=3.4, on the right, are given in Fig. 11 at the evaluation time.

The heat flux increases with axial position until the end of the combustion chambers and starts to approach a constant value just before the nozzle section. The heat flux peak values are about 6.8 MW/m^2 and 5.5 MW/m^2 at OF=2.2 for the round and rectangular hardware, respectively, and about 7.8 MW/m^2 and 6 MW/m^2 at OF=3.4. Differently from the pressure signal, the heat flux presents a plateau in the last section upstream the nozzle for all the mixture ratios tested. A constant heat flux level is reached in an earlier axial position for OF=2.2 than for other mixture ratios. A slight increase in the heat flux can be noticed with increasing mixture ratios and a similar trend has been observed for all tested pressure levels. Based on the pressure scaling method in Eq. 10, all heat flux data for OF=2.2 are scaled by $1/p_c^{0.8}$ and the results are shown in Fig. 12(a). It can be seen that the heat flux curves have the

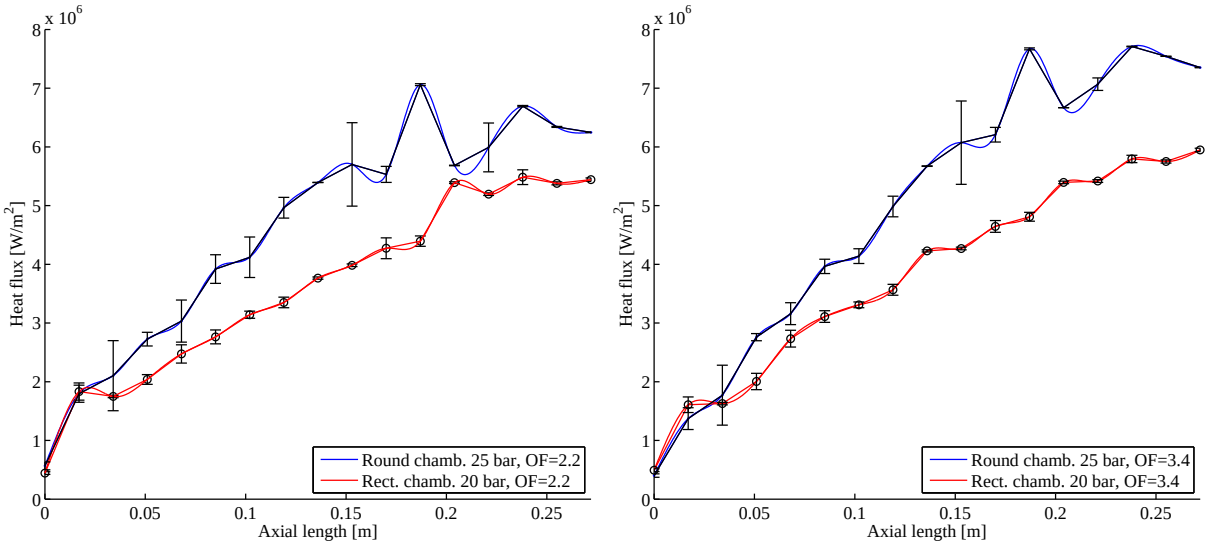

(a) OF=2.2 (b) OF=3.4

Figure 11: Axial heat flux distribution at p_c=20 bar and p_c=25 bar, respectively for the rectangular and round chamber

same qualitative trends but do not reach exactly the same values. As discussed in section 4.2.1, the heat flux level of the rectangular chamber is lower compared to the round chamber for the 20 bar case. In order to bring the heat flux profiles of the round chamber closer together, a different scaling exponent for the combustion chamber pressure has been applied. By using 0.44 as an exponent the heat flux profiles for 20 and 25 bar test case are almost identical, as shown in Fig. 12(b). However, this scaling equation can not be extrapolated to higher pressure levels without corresponding test data, which can not be obtained from the current set-ups, because to the temperature limits of the capacitive chamber segments. Currently, CFD simulations aiming for a better understanding of the boundary layer build-up are performed at the Institute and will be presented in future publications.

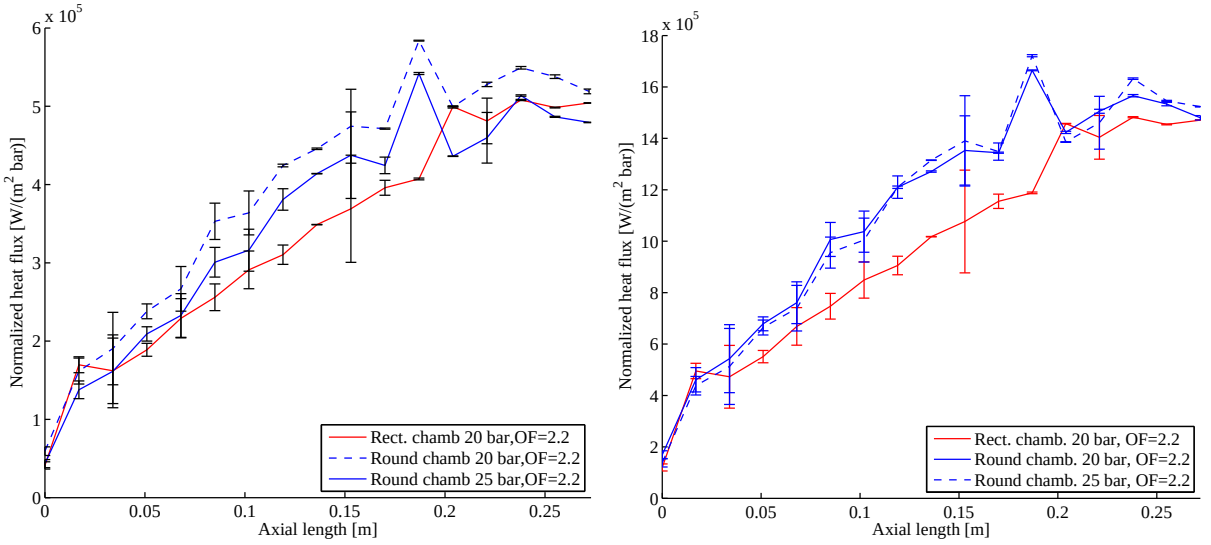

(a) $1/p_c^{0.8}$ (b) $1/p_c^{0.44}$

Figure 12: Heat flux normalized with chamber pressure

Due to higher chamber pressure in the round combustion chamber, higher temperature level can be expected for this approach. Although a higher heat flux is clearly detectable for the round combustion chamber, the level of the temperature readings are much closer to the rectangular chamber for this scaling approach. This is due to the non-

uniform distribution of the heat flux in the rectangular chamber and to the different amount of chamber cross sectional area, as already described in paragraph 4.2.1. The temperature of the round combustion chamber, which appears to be lower than in the rectangular combustion chamber for OF=2.2, becomes gradually higher with increasing mixture ratios. Generally, an increase in wall temperature, corresponding to the increase in heat flux, is visible at higher mixture ratios for both configurations.

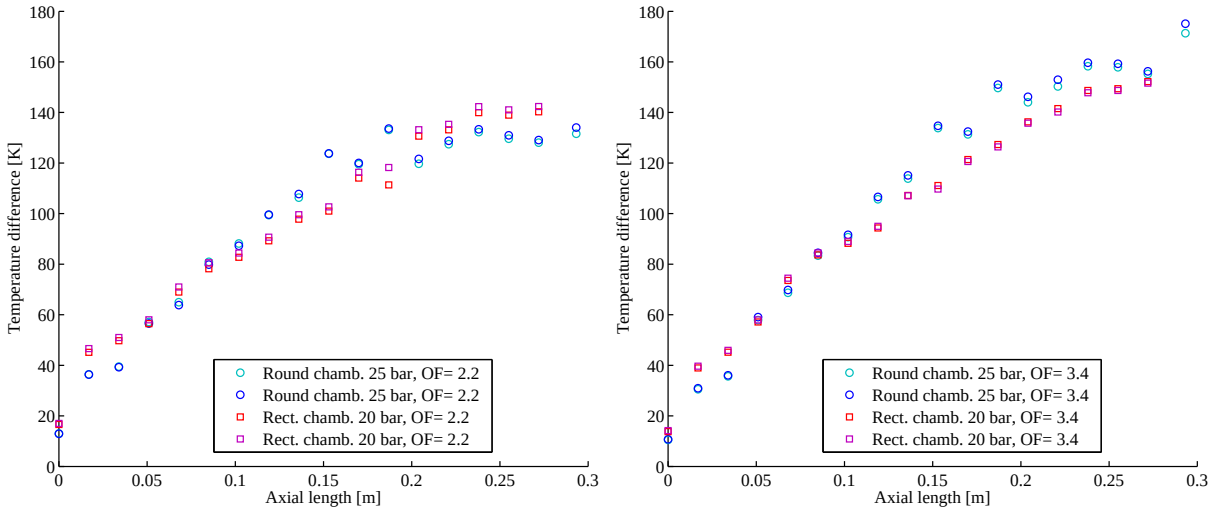

(a) OF=2.2 (b) OF=3.4

Figure 13: Wall temperature distribution at p_c=20 bar and p_c=25 bar, respectively for the rectangular and round chamber

4.4 Performance parameter

To describe the performance of an injector system, one of the parameters to look at is the combustion efficiency (η_{c^*}). The combustion efficiency is a measure of the effectiveness of a combustion chamber to convert the internal energy contained in the fuel into heat thermal energy for use by the process. Table 5 gives the values of the combustion efficiency for both the chambers at a mixture ratio equal to 2.2. Three approaches[13] are used to calculate the combustion efficiency. The adiabatic wall assumption (AW), in which the heat losses to the wall are not taken into consideration, the Jannaf[21] and LFA-Legacy method,[22] in which the theoretical characteristic velocity is corrected for the heat losses towards the chamber wall. While the LFA-Legacy method assumes equilibrium conditions, the Jannaf method assumes frozen condition at the combustion-end in order to recalculate the total conditions at the throat. Due to the similar physical combustion processes in the two combustion chambers a similar combustion efficiency is expected.

Table 5: Combustion efficiency at OF=2.2.

	p_c [bar]	Comb. Eff. (AW)	Comb. Eff. (LFA-Legacy)	Comb. Eff. (Jannaf)
Rect. chamb	20	0.950	0.976	0.976
Round chamb.	20	0.948	0.976	0.976
Round chamb.	25	0.965	0.988	0.988

In the first scaling approach, in which the combustion chamber pressure is mantained constant, a similar efficiency is obtained for the two chambers. For the second scaling approach, a higher efficiency value is obtained for the round combustion chamber, this has to be attributed to the higher chamber pressure obtained and not to a different physical phenomenon happening in the two chambers. While the combustion energy in the system is proportional to the combustion chamber pressure level, the losses in energy do not scale in a one to one proportion, and this results in a higher adiabatic wall efficiency for higher pressure levels. A recent study[7] on LOX/CH4 rocket engines for upper stage system at pressure ranges from 10 bar to 30 bar, have found that increasing chamber pressure results in decreasing kinetic losses and generally produces higher thrust performance. Moreover, the concentration of species has a strong impact at lower pressure levels. The increase of chamber pressure, from 20 to 25 bar, reduces the dissociation in

smaller species that could take energy away. When the pressure increases, the consumption of oxygen in the system is higher and the energy released by burning the propellant and the formation of lower energy carrier molecules can lead to higher combustion efficiency in the system.

5. Conclusion

In the context of the national research program Transregio SFB/TRR-40 on "Technological Foundations for the Design of Thermally and Mechanically Highly Loaded Components of Future Space Transportation Systems", two single element chambers using gaseous oxygen and gaseous methane are experimentally tested and compared at relevant rocket engine conditions. The two chambers mainly differ in their cross section, round and rectangular, and in their chamber wall thickness. Several parameters are mantained constant between the two combustion chambers to assure similarity of the combustion process. Since the injector element has the biggest influence on the performance and heat flux characteristics, in both combustion chamber configurations the injector elements is kept the same. The two chambers are compared under two scaling procedures. In the first scaling approach, where the combustion chamber pressure is mantained constant, similar heat flux levels and combustion performance are reached. Nevertheless, the integral heat flux level, obtained for the rectangular chamber, is slighthly lower compared to the round combustion chamber. This could be attributed to the effects given by the presence of the corners and the stronger recirculation zone in the rectangular chamber. As second approach, the mass flow rate at the injector are kept similar. Due to the different cross sectional area a higher pressure level in the round combustion chamber is obtained (smaller throat at constant contraction ratio). The higher pressure reached is directly correlated to higher heat flux and combustion chamber efficiency for the round combustion chamber. The differences in the hot wall surface and chamber wall material play a significant role in the thermal response of the hardware to a given heat flux level. A higher level of temperature would be obtained in the chamber having less heat capacity to disperse the heat for a total equal distribution of heat flux. The differences in chamber cross sectional area and chamber wall material lead to a different response in the temperature readings from a given heat flux on the chamber wall. Moreover, the presence of the corners lead to a not uniform distribution of the heat flux, having the maximum peak in the middle plane, where the thermocouple sensors are placed. Numerical simulations which aim to a better understanding of the influence of the different geometries in the combustion process are ongoing and will be presented in further publications.

Acknowledgments

Financial support has been provided by the German Research Foundation (Deutsche Forschungsgemeinschaft-DFG) in the framework of the Sonderforschungsbereich Transergio 40. The authors thank Nikolaos Perakis and Patrick Jiskra for their technical support during the test campaigns and the post processing of the data. The authors also would like to acknowledge the colleagues Christof Roth and Julian Pauw for the valuable discussions and interest.

References

[1] H. Burkhardt, M. Sippel, A. Herbertz, and J. Klevanski. Kerosene vs. methane: A propellant tradeoff for reusable liquid booster stages. *Journal of Spacecraft and Rockets*, 41(5):762–769, 2004.

[2] H.W Valler. Design, fabrication, and delivery of a high pressure lox-methane injector. *NASA CR-161343, Aerojet Liquid Rocket Company Report 33205F, Contract NASA-33205*, 1979.

[3] J. Locke, S. Pal, and R. Woodward. Chamber wall heat flux measurements for a LOX/CH4 propellant uni-element rocket. *AIAA 2007-5547*.

[4] A. Kootyev and L. Samoilov. New engines to power advanced launch vehicles. *Aerospace Journal*, 1998.

[5] J. Lux, D. Suslvov, M. Bechle, M. Oschwald, and O. Haidn. Investigation of sub- and supercritical LOX/Methane injection using optical diagnostics. *AIAA 2006-5077*.

[6] S. Zurbach, J.L. Thomas, P. Vuillermoz, L. Vingert, and M. Habiballah. Recent advances on LOX/Methane combustion for liquid rocket engine injector. AIAA 2002-4321, 2002.

[7] S. Ueda, T. Tomita, T. Onodera, Y. Kano, I. Kubota, and T. Munenaga. Hot-firing test of methane-fueled rocket engine under high altitude condition. *Joint Propulsion Conference & Exhibit*, (AIAA 2013-4056), 2013.

[8] R. Schuff, M. Maier, Sindiy, O., C Ulrich, and S. Fugger. Integrated modeling and analysis for a lox/methane expander cycle engine. *Joint Propulsion Conference & Exhibit*, AIAA 2006-4534, 2006.

[9] S.S Penner. On the development of rational scaling procedures for liquid-fuel rocket engines. *Journal of jet Propulsion*, 27(2):156–161, 1957.

[10] M.P Celano, S. Silvestri, G. Schlieben, C. Kirchberger, and O.J Haidn. Injector characterization for a gox-gch4 single element combustion chamber. *5th European Conference For Aeronautics and Sapce Sciences, (EUCASS) 2013*, 2013.

[11] S. Silvestri, M.P Celano, G. Schlieben, O. Knab, and O.J Haidn. Investigation on recess variation of a shear coaxial injector for a aingle element gox-gch4 combustion chamber. *6th European Conference for Space Sciences, (ISTS) 2015*, 2015.

[12] D. Suslov, A. Woschnak, J. Sender, and M. Oschwald. Test specimen design and measurement technique for investigation of heat transfer processes in cooling channels of rocket engines under real thermal conditions. *Joint Propulsion Conference & Exhibit*, (AIAA 2003-4613), 2003.

[13] S. Silvestri, M.P Celano, G. Schlieben, C. Kirchberger, and O.J Haidn. Characterization of a gox-gch4 single element combustion chamber. *Space Propulsion*, 2014.

[14] J. Hulka. Scaling of performance in liquid propellant rocket engine combustion devices. *AIAA 2008-5113*, 2003.

[15] R. Arnold, D. I. Suslov, and O.J Haidn. Film cooling in a high- pressure subscale combustion chamber. *Journal of Propulsion and Power*, 26(3):428–438, 2005.

[16] M.P. Celano, S. Silvestri, J. Pauw, N. Perakis, F. Schily, D. Suslov, and O.J. Haidn. Heat flux evaluation methods for a single element heat-sink chamber. *6th EUROPEAN CONFERENCE FOR AEROSPACE SCIENCES, (ISTS) 2015*, 2015.

[17] E. Artioukhine. Heat transfer and inverse analysis. *RTO-EN-AVT-117*, 2010.

[18] D. R. Bartz. A simple equation for rapid estimation of rocket nozzle convective heat transfer coefficients. *Journal of Jet Propulsion*, pages 49–51, 1957.

[19] F. P. Incropera, D. P. Dewitt, and T. L. Bergman. *Foundamentals of Heat and Mass Transfer*. 1981.

[20] G. Cai, W. Wang-wei, and T. Chen. *Method for Measurement of Single-Injector Heat Transfer Characteristics and Its Application in Studying Gas-Gas Injector Combustion Chamber*. 2011.

[21] C. Kirchberger, G. Schlieben, and O. J. Haidn. Assessment of film cooling characteristics in a GOX/Kerosene rocket combustion chamber. *Joint Propulsion Conference & Exhibit*, (AIAA 2013-4144), 2013.

[22] Johns Hopkins University. *Jannaf Rocket Engine Performance Test Data Acquisition and Interpretation Manual*. 1957.